Ann. Phys. (Berlin) **525**, No. 1–2, 135–142 (2013) / DOI 10.1002/andp.201200216

annalen der physik

Characterizing the optical near-field in the vicinity of a sharp metallic nanoprobe by angle-resolved electron kinetic energy spectroscopy

Doo Jae Park[1,2], *Björn Piglosiewicz*[1,2], *Slawa Schmidt*[1,2], *Heiko Kollmann*[1,2], *Manfred Mascheck*[1,2], *Petra Groß*[1,2], *and Christoph Lienau*[1,2,*]

Received 14 August 2012, revised 3 December 2012, accepted 4 December 2012
Published online 8 February 2013

The effect of the near-field distribution of sharply etched, nanometer-sized gold tapers on angle-resolved kinetic energy spectra of electrons photoemitted by ultrafast laser pulse irradiation is investigated both experimentally and theoretically. In the experiments, the enhancement of the local electric field at the tip apex is sufficiently large to enable optical field induced tunneling of electrons tunnel out of the metal tip. Strong field gradients near the tip apex, with a decay length shorter than the quiver amplitude, accelerate the electrons to high energies within less than one optical cycle. This electron emission is confined to a narrow cone angle around the taper axis, while low-energy quiver electrons cover a much broader angular range. This subcycle acceleration manifestly alters the energy distribution of the emitted electrons, resulting in pronounced plateaus in their kinetic energy spectra. The electron motion in the curved vectorial electric field is analyzed and it is shown that observed changes of both the kinetic energy spectra and their angular distribution depend sensitively on the near-field decay length and curvature, which indicates that such angle-resolved kinetic energy spectra of photoemitted electrons give information on the optical near-field distribution in the vicinity of nanometer-sized field emitters.

1 Introduction

Metallic nanostructures such as plasmonic nanoantennas [1, 2], nanoparticles [3], and sharply etched metallic nanoprobes [4, 5] are characterized by large optical field enhancement and strong spatial gradients of their near-field distribution. A number of applications have been developed based on these strong field gradients, such as plasmonic waveguides and devices [6] or near-field scanning optical microscopy (NSOM) with ultrahigh spatial resolution [5, 7–10]. Furthermore, due to the large field enhancement, it becomes relatively easy to create intense local electromagnetic fields, reaching or even exceeding the interatomic field, when irradiating such nanostructures with ultrashort pulses from low-power, high-repetition rate laser systems. This has recently enabled the study of a wealth of strong field photoemission phenomena in metallic nanostructures [9, 11–13] and dielectric nanospheres [14], including ponderomotive photoelectron acceleration and emission of extreme ultraviolet (EUV) radiation [15, 16].

Among such metallic nanostructures, sharply etched nanotapers are currently intensively studied as testbeds for exploring various strong-field phenomena in the photoemission of electrons [9, 12, 17–19]. The importance of such nanotips in this field is due to their large field enhancement, relatively simple geometry and rather well-controlled shape, which facilitates a theoretical modeling of the observed effects. Even though, so far, the vectorial electric field distribution around the tip apex could not yet be measured directly, it can be calculated using a variety of numerical simulation techniques [4] or existing analytical models based on a hyperboloidal tip shape [20, 21]. Such simulations show a short decay length l_F of the evanescent near-field, slightly less than the radius of curvature of the tip. When such a sharply etched nanoprobe is illuminated with intense few-cycle laser pulses with a near-infrared center wavelength, electrons can be photoemitted by different

* Corresponding author E-mail: christoph.lienau@uni-oldenburg.de
[1] Institut für Physik, Carl von Ossietzky Universität, 26129 Oldenburg, Germany
[2] Center of Interface Science, Carl von Ossietzky Universität, 26129 Oldenburg, Germany

physical mechanisms, including multiphoton ionization [9, 12], above-threshold ionization [17] and optical field emission [18, 19]. In the optical field emission regime, the local field at the tip apex is sufficiently large to transiently bend the vacuum potential and to let electrons tunnel out of the metal. These electrons are then accelerated within the temporally oscillating electric near-field of the tip and this acceleration manifestly alters the kinetic energy distribution of the photoemitted electrons. Electron acceleration becomes particularly interesting when the near-field decay length l_F is shorter than the quiver amplitude $l_q = e \cdot f \cdot E_0/(m\omega^2)$ of the photoemitted electrons, where E_0 denotes the amplitude of the incident laser field in the absence of the tip [19]. The laser frequency is ω, and e and m are the electron charge and rest mass, respectively. The factor f accounts for the local field enhancement induced by the gold tip, reaching values of $f \approx 10$ for sharp gold tips [9, 18]. In case that $l_q > l_F$, the net acceleration of the electrons is mostly acquired within the first half optical cycle after the release of the electron from the tip. This leads to a suppression of the traditional quiver motion of the electrons [22, 23] and to a strong modification of the shape and high-energy cutoff of the kinetic energy distribution [19]. Furthermore, the force exerted along curved field lines in the vicinity of the asymmetric nanotaper is expected to alter the electron's trajectories, thus changing the resultant emission direction of the electrons from the tip.

These findings suggest the possibility of a precise characterization of the local electric field, including its decay length, field line curvature and local field amplitude, by analyzing angle-resolved kinetic energy spectra of the electrons that are emitted from nanostructures. This would allow one to quantitatively correlate local electric field and the resulting optical nonlinearities [24], specifically the EUV or electron emission yield. Also this should be helpful in optimizing the geometrical shape of the nanostructures for their nonlinearities. In this report, we use angle-resolved kinetic energy spectroscopy to characterize the optical near-field distribution of sharp gold tapers with sub-10-nm radius of curvature. Marked changes in the kinetic energy spectra with increasing field amplitude, specifically the development of a broad plateau-like region in those spectra, are related to the acceleration of photoemitted electrons within the spatial gradient near the taper apex on a sub-cycle time scale. By comparing the shape of those spectra to two-dimensional simulations based on a modified Simpleman model, we characterize the decay length of the optical near-field. Variations in the kinetic energy spectra for different emission angles are associated with the field curvature in the vicinity of the tip.

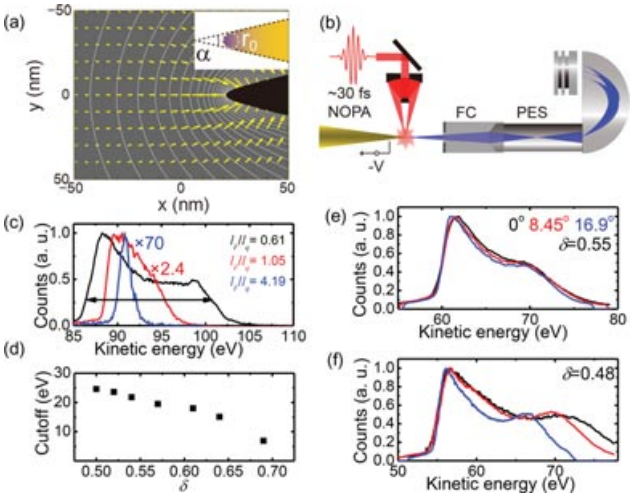

Figure 1 (online color at: www.ann-phys.org) Simulated equipotential and electric field lines in the vicinity of a hyperboloidal gold tip (inset) with radius $r_0 = 1.5$ nm and an opening angle α of 30°. (b) Schematic of the experimental setup. Ultrafast laser pulses from a non-collinear optical parametric amplifier with ~30 fs duration are focused onto a sharp gold tip with 10 nm tip radius inside a vacuum chamber. Angle-resolved kinetic energy spectra are recorded using a photo electron spectrometer (PES). A Faraday cage (FC) is mounted between tip and PES entrance to minimize static field line distortions. (c) Normalized angle-integrated spectra recorded using pulses with decay parameters $\delta = l_F/l_q = 0.61$, 1.05, and 2.65. A small negative bias of $U_B \sim 90$ eV is applied to the tip. The black arrow denotes the sum of cutoff energy U_c and U_B. (d) Width of the spectra as a function of $\delta = l_F/l_q$. For $\delta < 1$, the width increases gradually with decreasing δ. (e) Angle-resolved kinetic energy spectra at detection angles of $\theta_\infty = 0$ (black curve), 8.45° (red curve), and 16.9° (blue curve) for $\delta = 0.55$. No significant differences in spectral shape are observed. (f) Kinetic energy spectra at the same detection angles as in (e) for a larger quiver amplitude ($\delta = 0.48$). The width and cutoff energy increases at small angles. The spectra of (c), (e) and (f) are extracted from full angle-resolved sets of spectra reported in Ref. [26].

In the vicinity of sharply etched metal tips, the electric field distribution $\vec{E}(\vec{r})$ at a given instant in time is highly confined around the apex due to the interplay between the lightening rod effect and resonant plasmonic field enhancement [4, 9, 25]. By assuming a hyperboloid tip shape with a cone opening angle of $\alpha = 30°$ and a radius of the tip of $r_0 = 1.5$ nm (see inset of Fig. 1(a)), the equipotential lines can be calculated analytically as shown in Fig. 1(a) [20]. As expected from a nearly perfect metal surface (*i.e.*, a metal with a large but finite negative real part of the dielectric constant), the equipotential lines process nearly parallel to the tip

surface (black area in Fig. 1(a)). Correspondingly, the electric field vectors $\vec{E}(\vec{r})$ at the metal surface are almost normal to the surface (yellow arrows in Fig. 1(a)). The dense concentration of equipotential lines near the tip apex indicates the field enhancement and localization around the tip. An additional important feature is the curvature of the field lines due to the symmetry-breaking introduced by the tip. This field curvature strongly affects the motion of the electrons emitted from the metal surface which are accelerated within the local, temporally oscillating electric field distribution $\vec{E}(\vec{r}, t)$ according to Newton's equation of motion. Hence the electron trajectories and their terminal velocity $\vec{v}_\infty = \vec{v}(t \to \infty)$ after escaping from the strong field region carries important information on $\vec{E}(\vec{r}, t)$. Experimentally, we measure $\vec{v}_\infty$ by simultaneously recording the kinetic energy $E_{kin} = \frac{1}{2} m \vec{v}_\infty$ and the terminal emission angle $\theta_\infty = \arctan\left(\vec{v}_{y,\infty}/\vec{v}_{x,\infty}\right)$ of the photoemitted electrons.

2 Experimental setup

In the experiments, photoelectrons are generated by focusing ultrashort near-infrared (NIR) pulses from a non-collinear optical parametric amplifier (NOPA) with ~30 fs duration onto the tip. The metal tip is a sharply etched single crystalline gold taper mounted inside a vacuum chamber [26]. This new etching procedure [25] provides tips with a particularly smooth shaft surface and a small radius of curvature r_0 of less than 10 nm. The shape of the tip defines the field enhancement factor f and the near-field decay length l_F. In our experiments, we tune the wavelength of the laser pulses from 1.0 μm to 1.5 μm and their energy from 0.05 nJ to 1.2 nJ, effectively varying the quiver amplitude and thus the decay parameter $\delta = l_F / l_q$. To avoid pulse distortion, all-reflective optics are applied and a Cassegrain objective is used to achieve tight focusing down to 1.5 μm (Fig. 1(b)) [27]. Angle-resolved kinetic energy spectra are recorded with a photo-electron spectrometer (PES) equipped with a two-dimensional CCD detector. A Faraday cage (FC) is used to minimize static field distortions induced by nearby electrostatic objects, *i.e.*, the Cassegrain objective and the sample translation stages.

Angle-integrated photoemision spectra, normalized to their maximum value, are displayed in Fig. 1(c). The spectra have been recorded with pulse energies and center wavelengths of 0.05 nJ/1.0 μm ($f \cdot E_0 = 7.2$ V/nm, $\delta = 4.2$, blue curve), 0.2 nJ/1.4 μm ($f \cdot E_0 = 15$ V/nm $\delta = 1.1$, red curve [26]), and 0.6 nJ/1.4 μm ($f \cdot E_0 = 25.4$ V/nm, $\delta = 0.6$, black curve [26]), respectively. To compare different spectra, we plot them as a function of the decay parameter δ. Here we take values of $f \approx 9$ and $l_F \approx 1.5$nm, as these are found to best match our experimental results, as explained in detail below. During the measurements, a small negative bias of $U_B \sim 90$ eV has been applied to the tip to avoid static charging and undesired charged particle attachments during electron emission. For $\delta = 4.1$ we see a narrow spectrum as is typical for multiphoton ionization [26]. With decreasing δ, the spectrum broadens until a pronounced plateau develops which extends over more than 20 eV at the smallest decay parameter of $\delta = 0.61$. This field-induced broadening of the photoemission spectrum and the development of the plateau region are experimental signatures of optical field induced tunneling of electrons out of the metal tip and for a pronounced electron acceleration within the strong field gradient at the tip apex. We take the width of this plateau as the difference between the high-energy cutoff (at half plateau height, black arrow in Fig. 1(c)) and the low-energy cutoff. In Fig. 1(d), the plateau width is plotted as a function of the decay parameter showing a gradual decrease in width with increasing δ. We generally observe a clear broadening of the spectrum for $\delta < 1$, corresponding to a Keldysh parameter $\gamma = \omega\sqrt{2m\Phi}/(e \cdot f \cdot E_0)$ of about 0.8. We take a value of $\Phi = 5.5$ eV, which we consider a good estimate for the work function of our annealed tips [28]. Generally, the value $\gamma \approx 0.8$ agrees quite well with the usual Keldysh criterion for the transition between multiphoton and strong field emission [18]. Care should be taken, that this criterion has been derived for the tunnel ionization of atoms, in the absence of local field gradients. In case of metal nanostructures, however, the near field decreases quickly with increasing distance from the surface and this should in fact shift the transition to larger local field values. Our measurements indicate that both the spectral width and the shape of the spectra are strongly affected by the decay parameter $\delta = l_F / l_q$. The high-energy cutoff allows us to deduce a first estimate of the field enhancement factor f. For a planar metal film, this cutoff is given as twice the ponderomotive energy $U_P = (e \cdot f \cdot E_0)^2/(4m\omega^2)$, indicating $f \approx 7$. We will show below that for near-fields with a decay length of ~2 nm, the cutoff energy is reduced, to ~ 1.2 U_P, increasing the estimated value of the field enhancement factor to $f \approx 9$.

In order to study the effect of electron acceleration on their emission angles, angle-resolved kinetic energy spectra have been recorded at a fixed wavelength of 1.5 μm and with $U_B \sim 50$ eV. Measurements at detection angles of 0°, 8,45°, and 16.9° are plotted in Figs. 1(e) and (f) for $\delta = 0.55$ and $\delta = 0.48$, respectively. The data are extracted from a full set of angle-resolved spectra reported in Ref. [26], recorded for pulse energies of 0.9 nJ (Fig. 1(e))

and of 1.2 nJ (Fig. 1(f)). At the shorter quiver amplitude ($\delta = 0.55$) the spectra recorded are essentially independent of the detection angle. At the longer quiver amplitude ($\delta = 0.48$), however, a substantial change both in spectral shape as well as high-energy cutoff is observed between different detection angles, showing that higher energy electrons are predominantly detected at smaller emission angles. This gives evidence for a steering of the electron motion along the curved field lines and indicates that such steering effect becomes more pronounced at larger quiver amplitudes.

To account for the changes observed in the angle-resolved kinetic energy spectra we have performed numerical simulations of the electron trajectories within an extended semiclassical Simpleman model [17, 19]. We assume a two-dimensional hyperboloidal gold tip with an opening angle of $\alpha = 30^\circ$ and use existing analytical expressions to describe the temporally and spatially varying electric field $\vec{E}(\vec{r}, t) = \vec{E}(\vec{r}) \cdot T(t)$ as shown in Fig. 1(a) [20, 21]. The time dependence of the field is taken as $T(t) = \exp(-2\ln 2 \cdot t^2/\tau^2)\cos(\omega t)$ where τ denotes the experimentally measured pulse duration of 30 fs and ω the carrier frequency. A Fowler-Nordheim equation [19, 29] neglecting field-dependent barrier suppression and assuming electron generation only during negative half-cycles (electron acceleration away from the tip) describes the tunneling probability $p(t)$ as a function of the birth time $t = \varphi/\omega$ of the electron (φ: emission phase) as follows:

$$p(t) = \Theta(E(t))\frac{e^3 E(t)^2}{16\pi^2\hbar\Phi}\exp\left(-\frac{4\sqrt{2m}\Phi^{3/2}}{3\hbar e E(t)}\right). \quad (1)$$

Here, $\hbar$ is the reduced Planck constant and $\Theta(E(t))$ the Heaviside step function. After the birth of the electron, its motion under the action of the force field $\vec{F}(\vec{r}, t) = q \cdot \vec{E}(\vec{r}, t)$ is simulated by solving the classical equation of motion and kinetic energy spectra are generated by averaging over a distribution of emission phases and sites. It is assumed that electrons recolliding with the tip are perfectly reflected. Such a model has recently successfully been used to describe different strong-field photoemission phenomena [17, 19] and successfully been tested against different more refined approaches [30]. In such a model, the high-energy cutoff of the spectrum is predominantly defined by the ponderomotive potential [19] while the shape of the spectrum, in particular the amplitude and form of the plateau region, largely depends on l_F.

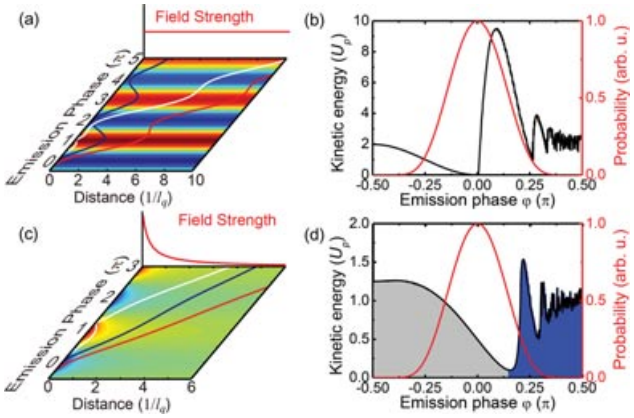

Figure 2 (online color at: www.ann-phys.org) (a) Simulated trajectories of electrons emitted at different phases of the laser field of $\varphi = -0.25\,\pi$ (red curve), 0 (black curve), and $0.25\,\pi$ (white curve), in a spatially homogeneous, temporally oscillating electric field (field strength color-coded). The laser wavelength is $1.5\ \mu$m and E_0 is set to 25.4 V/nm, giving a quiver amplitude of 2.8 nm. Quiver motion is observed for emission phases of $-0.25\,\pi$ and $0\,\pi$. At $0\,\pi$, the electron does not escape from the metal surface. Rescattering at the tip surface is observed at $0.25\,\pi$. (b) Calculated terminal kinetic energy distribution (black curve) and generation probability (red curve) as a function of the emission phase φ. Electrons are in the quiver regime for $\varphi < 0$ and rescattering is observed at $\varphi > 0$. (c) Simulated electron trajectories in the near-field of a sharp metal tip with $r_0 = 1.5$ nm and $\alpha = 30^\circ$ at different φ. The peak electric field at the tip surface is $E_0 = 25.4$ V/nm. Sub-cycle acceleration is seen at $\varphi = -0.25\,\pi$ and 0 (red and black curve, respectively), whereas rescattering occurs at $\varphi = 0.25\,\pi$ (white curve). (d) Calculated terminal kinetic energy distribution (black curve) and generation probability (red curve) as a function of φ. Electrons are in the sub-cycle regime for $\varphi < 0.14\,\pi$ (gray shaded area) and in the quiver regime for larger emission phases (blue shaded area).

3 Discussion

We first consider electron acceleration in a temporally oscillating, but spatially homogeneous electric field, as is common, *e.g.*, in high harmonic generation from atomic systems [22]. We choose a laser wavelength of $1.5\ \mu$m and $\vec{E}(\vec{r}) = E_0 = 25.4$ V/nm, corresponding to $l_q = 2.8$ nm. The pulse duration is set to $\tau = 30$ fs. In this case, most electrons are in the quiver regime, as can be seen from the three representative trajectories plotted in Fig. 2(a), calculated for emission phases $\varphi = -0.25\,\pi$, $0\,\pi$, and $0.25\,\pi$. For negative emission phases, the electrons undergo a quiver motion (red curve in Fig. 2(a)), with a total kinetic energy which reaches a maximum $2\,U_p$ at

$\varphi = -0.5\ \pi$ and decreases to zero for an emission phase of 0. Here, forward and backward acceleration cancel out and the electron cannot depart from the surface (blue curve in Fig. 2(a)). The terminal kinetic energy is plotted in Fig. 2(b) as a function of the emission phase (black curve). In electron trajectories with positive emission phases, one or more rescattering events with the metal surface occur (see example trajectory for $\varphi = 0.25\ \pi$ as white curve). In our simulations, such recollisions are considered as being perfectly elastic and occurring at the tip surface. Such scattering events lead to a more complicated kinetic energy distribution in Fig. 2(b), as theoretically discussed, *e.g.*, in Ref. [14]. The terminal kinetic energy distribution shows a minimum at $\varphi = 0$, with zero kinetic energy corresponding to those electrons that cannot depart from the surface. When plotted together with the generation probability as a function of the emission phase, calculated using the Eq. (1) (red curve in Fig. 2(b)), this shows that the electrons with the highest generation probability possess the lowest kinetic energy, hence the shape of the kinetic energy spectrum is similar to an exponential decay function.

In Fig. 2(c), these results are compared to trajectory simulations for electrons emitted from the apex of a sharp metal tip with geometric parameters of $\alpha = 30^\circ$ and $r_0 = 1.5$ nm. For such a tip, the near-field decay length is $l_F \approx 1.5$ nm. The time structure of $\vec{E}(\vec{r}, t)$ is the same as that in Fig. 2(a) and the maximum field amplitude at the tip apex is $E_0 = 25.4$ V/nm, corresponding to $l_q = 2.8$ nm and $\delta = 0.54$. In case of such a strong field gradient, electrons emitted at a phase of $-0.25\ \pi$ (red curve) escape quickly from the strong field region within one half cycle of the laser oscillation. This rapid escape results in a complete suppression of the quiver motion since the electrons reach a low field region before they can be back-accelerated towards the tip surface. Due to this strong spatial inhomogeneity of the field there is no trajectory for which forward and backward motion cancel out exactly, which results in two major changes of the kinetic energy distribution plotted in Fig. 2(d). First, there is no emission phase for which the terminal kinetic energy is zero, and second, the phase of minimum kinetic energy $\varphi_{\min}$ is shifted away from $\varphi = 0$ to positive phases. Also the second effect is readily understood. The magnitude of the initial forward acceleration ($a > 0$), away from the tip surface, is much larger than during backward acceleration, requiring a shortening of the initial forward acceleration phase, and thus a shift in $\varphi_{\min}$ towards positive values, in order to approximately balance forward and backward motion. Therefore, the kinetic energy minimum does not coincide any more with the maximum generation probability. Also, the maximum kinetic energy ($\sim 1.5\ U_p$) is substantially reduced in comparison to the cutoff energy of $\sim 10\ U_p$ for a spatially homogeneous field. The strong field gradient limits the effective acceleration distance and this reduces the maxmimum kinetic energy gained by near-field acceleration. This shift in $\varphi_{\min}$ has interesting consequences. It greatly reduces the probability to generate recolliding electrons and also reduces the velocity of these electrons when recolliding with the tip surface. This suppression of recollision suggest that phenomena associated with these recolliding electrons such as, e.g., high harmonic generation [15,16], are actually suppressed in nanostructures with strong field gradients.

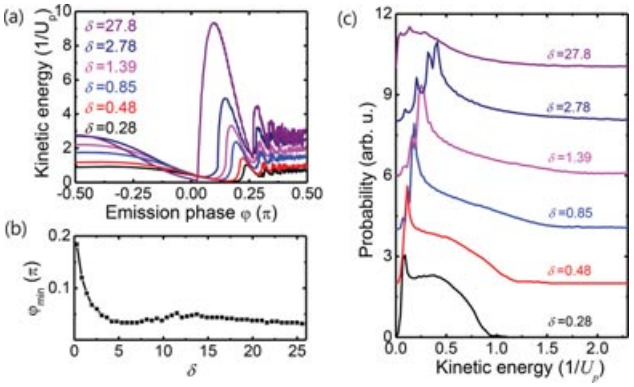

Figure 3 (online color at: www.ann-phys.org) (a) Calculated terminal kinetic energy distribution for different decay lengths l_F of the optical near-field and a fixed quiver amplitude of $l_q = 3.1$ nm. The laser wavelength is 1.5 μm and the peak electric field amplitude is 28.0 V/nm. The minimum kinetic energy shifts to larger emission phases as the decay length decreases. (b) Emission phase $\varphi_{\min}$ at minimum kinetic energy as a function of decay parameters $\delta = l_F / l_q$. (c) Calculated angle-integrated spectra for different δ, obtained by averaging kinetic energy distributions over a range of emission sites near the tip apex. The spectra are vertically shifted for clarity.

These two examples demonstrate that the suppression of quiver motion and strong-field acceleration of electrons in near-field gradients depend critically on the decay parameter δ, which is the only parameter that was changed from Fig. 2(a) to (c) (from ∞ to 0.54). This is investigated in more detail in Fig. 3(a), plotting the calculated kinetic energy distribution as a function of the emission phase for a number of different decay parameters $\delta = l_F / l_q$ ranging from 0.26 to 27.6. The quiver amplitude and the laser wavelength are fixed at 3.1 nm and 1.5 μm, respectively. As the decay parameter δ decreases, the maximum kinetic energy acquired in the presence and absence of recollisions decreases monotonically, effectively reducing the high-energy cutoff due to the reduction in field decay length and thus

acceleration distance. Also, the emission phase $\varphi_{\min}$ at the kinetic energy minimum increases with decreasing δ and therefore the total width of the kinetic energy distribution becomes much narrower. A plot of $\varphi_{\min}$ as a function of decay length (Fig. 3(b)) shows that $\varphi_{\min}$ shifts rapidly for $l_F < 2.5\, l_q$, and is almost constant at larger decay lengths, except for a small bump near $l_F = 10 \cdot l_q$.

The effect of the reduction in near-field decay length on the kinetic energy spectra is illustrated in Fig. 3(c). Angle-integrated spectra are calculated as a weighted average of the kinetic energy distribution from a range of emission sites on the tip surface. The decay parameter is varied by changing the radius of curvature of the tip, while keeping all other simulation parameters the same as in Fig. 3(a). It is evident that spatial field gradients have a pronounced effect on the kinetic energy spectra. With decreasing δ, the contribution of fast electrons to the spectrum increases considerably and, as in the experiment, a clear plateau-like high region develops for the shortest decay parameter, $\delta = 0.28$. This plateau only appears for decay lengths of the near-field much shorter than the quiver amplitude and quickly becomes fainter as δ increases. It is not discernible any more at $\delta = 1.39$, where the spectral shape simply follows an exponential decay. Additional peaks in the lower energy regions denote those electrons that are generated in the trailing edge of the laser pulse, which gain less kinetic energy due to the reduced electric field strength. Clearly, the shape of the kinetic energy spectra, specifically the presence or absence of the plateau region, provides a sensitive measure for the decay length of the optical near-field in the vicinity of the electron emitting nanostructure. The sensitivity is largest when the decay length approximately equals the quiver amplitude ($\delta \approx 1$). In this case, l_F is determined with an accuracy of much less than the quiver amplitude, up to ~3 nm under our experimental conditions. In order to approximately reproduce the shape of the spectra in Fig. 1, we need to assume a decay length of ~2 nm, even shorter than the tip radius deduced from SEM images [26]. Other parameters, such as the precise value of the work function, have only a minor effect on the shape of the kinetic energy spectra. This allows us to estimate the decay length of the near field from the shape of the experimental kinetic energy spectra. Knowing this value of the decay length we can now deduce a refined estimate of the field enhancement factor. The simulations in Fig. 3(c) predict that for $\delta \approx 0.6$ the cutoff energy is approximately $1 \cdot U_p$. From the corresponding spectrum in Fig. 1(c) we then deduce $f \approx 9$.

From the discussion above we expect that the field curvature not only influences the kinetic energy distribution of the emitted electrons, but also emission direction θ_∞ of the photoemitted electrons. This should result in pronounced changes in the angle-resolved kinetic energy spectra, if they are recorded at different detection angles. Experimentally, this is demonstrated in Figs. 1(e) and (f). In order to analyze the effect of near-field gradients on these spectra, we have simulated electron trajectories exemplarily for two different tip radii using the same simulation parameters as in Fig. 3. For a tip with a small radius of r_0 =1.0 nm which corresponds to a decay parameter of $\delta = 0.28$ (Fig 4(a)), the field lines are strongly curved (see the vectorial electric field distribution displayed as black arrows). In such a strongly curved field, the trajectories of the faster electrons (emitted at $\varphi = -0.25\,\pi$, red curve in Figs. 4(a) and (b)) differ substantially from those of the slower electrons (emitted at $\varphi_{\min} = 0.16\,\pi$, blue curve in Figs. 4(a) and (b)). The slow electrons hardly advance through the near-field region within one cycle of the laser oscillation and hence are driven *away* from the tip center by the curved, backward electric force. Electrons with a high kinetic energy

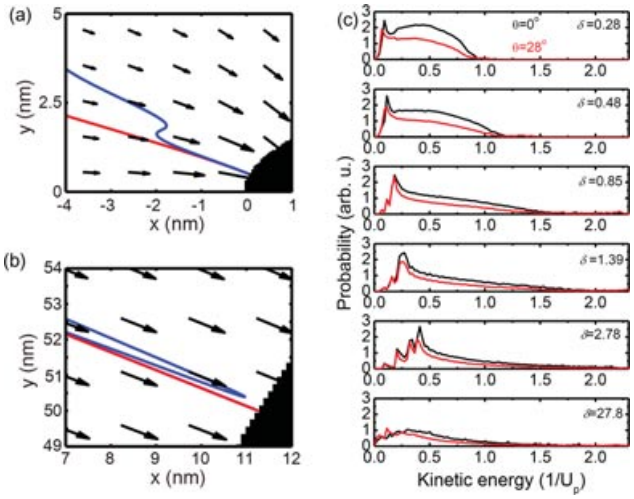

Figure 4 (online color at: www.ann-phys.org) (a,b) Snapshots of two representative electron trajectories of sub-cycle electrons ($\varphi = -0.5\,\pi$, red trajectories) and quiver electrons emitted at $\varphi = \varphi_{\min}$ (blue trajectories), from a site offset by ($\Delta x = 0.5 \cdot r_0$, $\Delta y \sim r_0(1 - \sqrt{3}/2)$) from the tip apex at the origin. The vectorial electric field distribution in the vicinity of the tip apex (black solid) is indicated by black arrows. The trajectories are calculated for two different tip radii, (a) $r_0 = 1.0$ nm ($\varphi_{\min} = 0.16\,\pi$), and (b) $r_0 = 100$ nm ($\varphi_{\min} = 0.02\,\pi$). (c) Angle-resolved spectra at detection angles of $\theta_\infty = 0°$ (black curve) and $\theta_\infty = 28°$ (red curve), for different decay parameters $\delta = l_F / l_q = 0.28$ to 28. The spectral shapes are very similar for large decay parameters $\delta \geq 1.39$, but show differences for small δ. Specifically, a much more pronounced plateau can be seen at the smaller detection angle for the smallest δ of 0.28.

escape from the strong field region within one half cycle of the laser oscillation. These electrons are therefore guided along the field lines and thus *towards* the tip center, which is in stark contrast to the dynamics of the electrons with a low kinetic energy. Both our experimental and theoretical observations are clear indications for a field-induced steering of highly near-field accelerated electrons towards the tip center.

This steering effect, however, is pronounced only for small decay parameters. When increasing δ beyond unity, the field curvature is reduced and the trajectories of faster and slower electrons resemble each other more closely. An example is shown in Fig. 4(b), displaying trajectories for a fast electron ($\varphi = -0.2\ \pi$, red curve) and an electron with minimum kinetic energy ($\varphi = 0.02\ \pi$, blue curve) for a tip with $r_0 = 100$ nm and $\delta = 27.8$. In this case, for the slowest electron, the off-axis drift per optical cycle is negligibly small, and hence the terminal emission angle hardly differs from that of the faster electron.

In Fig. 4(c), angle-resolved kinetic energy spectra are shown for various decay parameters ranging from $\delta =$ 0.28 to 27.8 (top to bottom). The spectra are displayed for two different detection angles, namely $\theta_\infty = 0^\circ$ (black curves) and $\theta_\infty = 28^\circ$ (red curves), and have been calculated for different decay parameters of $\delta = 0.28$ to 27.8 (top to bottom). Only for the smallest decay parameter the highly accelerated electrons concentrate around $\theta_\infty = 0$, giving evidence for the discussed field-induced steering. As the decay parameter increases, this effect becomes less pronounced, so that the spectra for different detection angles are very similar and resemble a simple exponential decay function for $\delta > 1.39$. The observation of clearly angle-dependent kinetic energy spectra in Fig. 1(f) therefore provides additional evidence that these measurements probe the strong field acceleration of photoemitted electrons within extremely steep near-field gradients in the vicinity of a very sharp gold tip. Their analysis confirms an estimate of a decay length of the optical near-field of only about 2 nm, even sharper than the measured radius of curvature of those tips of about 7 nm [26].

4 Summary

In summary, we have studied, both experimentally and theoretically, angle-resolved strong-field photoelectron spectra emitted from sharply etched metallic nanoprobes. Plateau-like kinetic energy spectra displaying a pronounced angle dependence are taken as a signature for the acceleration of the photoemitted electrons within the local near-field of the taper on a subcycle time scale. Calculations based on a modified two-dimensional Simpleman model indicate that the width and shape of angle-integrated spectra is a sensitive probe of the local near-field distribution, in particular in the limit when the quiver amplitude exceeds the near-field decay length. In this limit, angle-resolved kinetic energy spectra are sensitively dependent on the curvature of the field lines, indicating that such spectra can be taken as a new tool to characterize the local vectorial electric field distribution in the vicinity of metallic nanostructures. In the present work, we have used this concept to probe the near-field of a sharp gold tip and more work is currently underway to extend this experimental approach to other types of optical field emitters. We expect that this will provide an improved understanding of the strong-field driven electron dynamics in solid state nanostructures which will be helpful for the generation of intense ultrashort electron pulses or for optimizing optical nonlinearities of such nanostructures.

Acknowledgements. Financial support of the work by the Deutsche Forschungsgemeinschaft (SPP1391 and DFG-NSF Materials World Network), the Korea Foundation for International Cooperation of Science and Technology (Global Research Laboratory project, K20815000003) and the European Union (CRONOS) is gratefully acknowledged. D.J.P. wishes to thank the Hanse-Wissenschaftskolleg for a personal fellowship. The authors would like to thank P. Schreip for valuable discussions.

Key words. ultrafast nano-optics, strong-field photoemission, electron kinetic energy spectrum, metal nanostructure, optical near-field.

References

[1] P. Mühlschlegel, H. J. Eisler, O. J. F. Martin, B. Hecht, and D. W. Pohl, Science **308**, 1607–1609 (2005).
[2] P. J. Schuck, D. P. Fromm, A. Sundaramurthy, G. S. Kino, and W. E. Moerner, Phys. Rev. Lett. **94**, 017402 (2005).
[3] T. Klar, M. Perner, S. Grosse, G. von Plessen, W. Spirkl, and J. Feldmann, Phys. Rev. Lett. **80**, 4249–4252 (1998).
[4] A. Bouhelier, M. Beversluis, A. Hartschuh, and L. Novotny, Phys. Rev. Lett. **90**, 013903 (2003).
[5] D. Sadiq, J. Shirdel, J. S. Lee, E. Selishcheva, N. Park, and C. Lienau, Nano Lett. **11**, 1609–1613 (2011).
[6] S. I. Bozhevolnyi, V. S. Volkov, E. Devaux, J.-Y. Laluet, and T. W. Ebbesen, Nature **440**, 508–511 (2006).
[7] D. Richards, Philos. Trans. R. Soc. Lond. A **361**, 2843–2857 (2003).

[8] C. C. Neacsu, S. Berweger, R. L. Olmon, L. V. Saraf, C. Ropers, and M. B. Raschke, Nano Lett. **10**, 592–596 (2010).
[9] C. Ropers, D. R. Solli, C. P. Schulz, C. Lienau, and T. Elsaesser, Phys. Rev. Lett. **98**, 043907 (2007).
[10] C. Hoppener, Z. J. Lapin, P. Bharadwaj, and L. Novotny, Phys. Rev. Lett. **109**, 017402 (2012).
[11] J. Kupersztych, P. Monchicourt, and M. Raynaud, Phys. Rev. Lett. **86**, 5180–5183 (2001).
[12] P. Hommelhoff, C. Kealhofer, and M. A. Kasevich, Phys. Rev. Lett. **97**, 247402 (2006).
[13] P. Hommelhoff, Y. Sortais, A. Aghajani-Talesh, and M. A. Kasevich, Phys. Rev. Lett. **96**, 077401 (2006).
[14] S. Zherebtsov, T. Fennel, J. Plenge, E. Antonsson, I. Znakovskaya, A. Wirth, O. Herrwerth, F. Süßmann, C. Peltz, I. Ahmad, S. A. Trushin, V. Pervak, S. Karsch, M. J. J. Vrakking, B. Langer, C. Graf, M. I. Stockman, F. Krausz, E. Rühl, and M. F. Kling, Nature Phys. **7**, 656–662 (2011).
[15] S. Kim, J. Jin, Y.-J. Kim, I.-Y. Park, Y. Kim, and S.-W. Kim, Nature **453**, 757–760 (2008).
[16] M. Sivis, M. Duwe, B. Abel, and C. Ropers, Nature **485**, E1–E2 (2012).
[17] M. Krüger, M. Schenk, and P. Hommelhoff, Nature **475**, 78–81 (2011).
[18] R. Bormann, M. Gulde, A. Weismann, S. Yalunin, and C. Ropers, Phys. Rev. Lett. **105**, 147601 (2010).
[19] G. Herink, D. R. Solli, M. Gulde, and C. Ropers, Nature **483**, 190–193 (2012).
[20] N. Behr and M. B. Raschke, J. Phys. Chem. C **112**, 3766–3773 (2008).
[21] W. Denk and D. W. Pohl, J. Vac. Sci. Technol. B **9**, 510–513 (1991).
[22] P. B. Corkum, Phys. Rev. Lett. **71**, 1994–1997 (1993).
[23] G. Paulus, F. Grasbon, H. Walther, R. Kopold, and W. Becker, Phys. Rev. A **64**, 021401 (2001).
[24] T. Hanke, G. Krauss, D. Trautlein, B. Wild, R. Bratschitsch, and A. Leitenstorfer, Phys. Rev. Lett. **103**, 257404 (2009).
[25] S. Schmidt, B. Piglosiewicz, D. Sadiq, J. Shirdel, J. S. Lee, P. Vasa, N. Park, D. S. Kim, and C. Lienau, ACS Nano **6**, 6040–6048 (2012).
[26] D. J. Park, B. Piglosiewicz, S. Schmidt, H. Kollmann, M. Mascheck, and C. Lienau, Phys. Rev. Lett. **109**, 244803 (2012).
[27] B. Piglosiewicz, D. Sadiq, M. Mascheck, S. Schmidt, M. Silies, P. Vasa, and C. Lienau, Opt. Express **19**, 14451–14463 (2011).
[28] W. M. H. Sachtler, G. J. H. Dorgelo, and A. A. Holscher, Surf. Sci. **5**, 221–229 (1966).
[29] E. L. Murphy and R. H. Good, Phys. Rev. **102**, 1464–1473 (1956).
[30] S. Yalunin, M. Gulde, and C. Ropers, Physical Review B **84**, 195426 (2011).